ACS APPLIED MATERIALS & INTERFACES

Research Article

www.acsami.org

Self-Assembly of Monodisperse Starburst Carbon Spheres into Hierarchically Organized Nanostructured Supercapacitor Electrodes

Sung-Kon Kim,[†,⊥] Euiyeon Jung,[†,⊥] Matthew D. Goodman,[†] Kenneth S. Schweizer,[†] Narihito Tatsuda,[‡] Kazuhisa Yano,*[,‡,§] and Paul V. Braun*[,†]

[†]Department of Materials Science and Engineering and Frederick Seitz Materials Research Laboratory, University of Illinois at Urbana−Champaign, Urbana, Illinois 61801, United States

[‡]Inorganic Materials Laboratory, Toyota Central R&D Laboratories. Inc, Nagakute, Aichi 480−1192, Japan

[§]Materials Research Laboratory, Toyota Research Institute North America, 1555 Woodridge Ave., Ann Arbor, Michigan 48105, United States

Supporting Information

ABSTRACT: We report a three-dimensional (3D) porous carbon electrode containing both nanoscale and microscale porosity, which has been hierarchically organized to provide efficient ion and electron transport. The electrode organization is provided via the colloidal self-assembly of monodisperse starburst carbon spheres (MSCSs). The periodic close-packing of the MSCSs provides continuous pores inside the 3D structure that facilitate ion and electron transport (electrode electrical conductivity ∼0.35 S m^{-1}), and the internal meso- and micropores of the MSCS provide a good specific capacitance. The capacitance of the 3D-ordered porous MSCS electrode is ∼58 F g^{-1} at 0.58 A g^{-1}, 48% larger than that of disordered MSCS electrode at the same rate. At 1 A g^{-1} the capacitance of the ordered electrode is 57 F g^{-1} (95% of the 0.24 A g^{-1} value), which is 64% greater than the capacitance of the disordered electrode at the same rate. The ordered electrode preserves 95% of its initial capacitance after 4000 charging/discharging cycles.

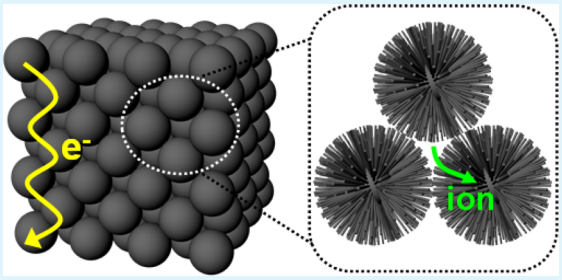

KEYWORDS: *supercapacitor, hierarchical structure, porous carbon, energy storage, colloid*

INTRODUCTION

The need for better electrical energy storage technologies drives considerable research on both batteries and supercapacitors (SCs). SCs, also known as electrochemical capacitors, are drawing particular attention for complementing or replacing conventional capacitors or batteries due to their high power capability, high round-trip efficiency, long-term cycle life (up to million charge−discharge cycles), low manufacturing cost, and intrinsic safety.[1] Advancements in carbon nanomaterials, such as graphene, carbon nanotubes (CNTs), and mesoporous carbon, all of which exhibit large surface areas, high electrical conductivities, and good chemical stabilities, are leading to considerable interest in using these nanomaterials for SC applications.[2,3] Since SCs store energy by reversible adsorption of ions from the electrolyte onto the active electrode materials concurrent with electron transport through the electrode, both the electrode's electrical conductivity and surface area are important. Thus, electrode architecture optimization is important because it can control the ion and electron kinetics and the total surface area.[4,5] Not surprisingly, there is a tradeoff between power density (determined by electron and ion conductivity) and energy density (determined by the total surface area) since maximizing surface area requires small average pore diameters, which tends to impede ion transport.[6,7] One emerging trend in SCs is to construct three-dimensional (3D) porous architectures with optimized pore networks that minimize electron and ion transport distances while maximizing the surface area per unit volume.[7−9]

3D porous electrodes for both SCs and batteries have been typically fabricated by mixing powdery porous materials with organic binder,[10−14] template-assisted,[15−27] and template-free (self-assembly) methods.[28−32] Although template-assisted methods can produce well-ordered electrode structures, it is challenging to provide a high volumetric energy density using a template method, since the template, which is fugitive, leaves large pores in the structure.[15,33] A well-ordered pore network is important for effective ion transport since when the micro-, meso-, or macropores are not well-interconnected there is a high electrolyte-induced ohmic resistance and the possibility of incomplete wetting of the electrode surface by electrolyte, resulting in a large potential drop (*IR* drop) and a decrease of ion-accessible surface area at high currents.[6,7,14,34] For example, although conventional activated carbon has large surface area (1700 m^2 g^{-1}) and good electrical conductivity, its capacity is only 10−20% of its theoretical value due to the long diffusion

Received: February 5, 2015
Accepted: April 13, 2015
Published: April 13, 2015

ACS Publications © 2015 American Chemical Society

DOI: 10.1021/acsami.5b01147
ACS Appl. Mater. Interfaces 2015, 7, 9128−9133

distances (>5 um) and high ion transfer resistance caused by its poorly defined pore structure.[13,35] Here, using hierarchically porous 3D SC electrodes formed from monodisperse starburst carbon spheres (MSCSs), we start to unravel the complex interplay between the electrode mesostructure and the properties of SCs. The system is template-free, because the self-assembling MSCSs are the active material, and the electrical conductivity of the electrode can be changed without changing the porosity of the MSCS, since the conductivity is a function of the degree of order (number sphere−sphere contact points) in the self-assembled MSCSs. The MSCSs have a large specific surface area (1260 m^2 g^{-1}, Supporting Information Table S1 and Figure S1), and thus a good specific capacity, and radially aligned micro- and mesopores that facilitate ion transport.[36] When assembled into a regular array, effective ion transport through the micro-, meso-, and macropores and efficient electron transport through the contacting MSCSs is observed. When the structure is disordered, the performance decreases, due to increases in the electrical resistivity and ion diffusion lengths in the structure.

EXPERIMENTAL SECTION

Fabrication of Monodisperse Starburst Carbon Spheres Electrodes. MSCSs and their colloidal assemblies were prepared as previously reported.[37,38] Briefly, MSCSs were oxidized in a Lindberg Furnace at 400 °C for 30 min in air. MSCSs (0.0053 g) were dispersed in ethanol (conc. 0.75 wt %) with ultrasonication for 4 h. Gold (80 nm)/chromium (8 nm) deposited silicon substrate was piranha cleaned (3:1 ratio of H_2SO_4/H_2O_2, v/v) for 40 min, followed by rinsing with Millipore water and then immersed in 50 mL of Milipore water with 0.5 g of 3-mercapto-1-propanesulfonic acid and sodium salt (Aldrich) for 12 h. The substrate was rinsed with Millipore water and then dried under a gentle stream of nitrogen gas. The substrate was positioned at a 20° angle in a 20 mL scintillation vial containing the oxidized MSCS suspension. The vial was placed in an incubator (Fisher, Isotemp 125D) and left at 40 °C for 24 h, followed by further drying at 150 °C for 1 h to ensure solvent removal. (As shown in Supporting Information Figure S2, the higher temperature drying step is necessary for complete solvent removal.) MSCSs with disordered structure were prepared using the same procedure, except the solvent was 1-butanol.

Characterization. Nitrogen adsorption−desorption isotherms, pore size, Brunauer−Emmett−Teller (BET) specific surface area, and pore volume were measured as previously described.[37] Mass of MSCS was recorded by Q50 thermal gravimetric analysis (TGA) in air. After electrochemical tests, samples were scraped off the substrate and transferred to an alumina sample cup for TGA measurements (Supporting Information Figure S3). Area of MSCS electrodes was measured by AmScope MT optical microscope and calculated using ImageJ. The microstructures were imaged using a Hitachi S-4700 SEM. Particle size distribution and zeta-potential measurements were conducted using a NICOMP 380 ZLS Particle Sizer. Electrochemical characterizations, including cyclic voltammetry (CV), galvanostatic charge/discharge (GCD), and electrochemical impedance spectroscopy (EIS), were performed using a VMP3 multichannel potentiostat (VMP3, Bio-Logic, USA) in the two-electrode mode at room temperature. Two electrodes were placed facing each other 0.5 cm apart in the 1 M Na_2SO_4 aqueous electrolyte. In the GCD profiles, the specific capacitance can be estimated using the following equation:

$$C = 2I/[(\Delta V/\Delta t)m] \quad (1)$$

where I is the current applied, $\Delta V/\Delta t$ is the slope of the discharge curve after IR drop at the beginning of the discharge curve, and m is the mass of electrodes. Electrical conductivity was measured using a four-point probe.

RESULTS AND DISCUSSION

The 3D-ordered MSCS electrode, abbreviated as MSCS-O, was created by first slightly oxidizing the MSCSs at 400 °C for 30 min in air, imparting a negative surface charge (−9.3 mV), probably due to the presence of oxygen-containing moieties, that is, hydroxyls, quinones, and carboxylic acids (Supporting Information Table S1).[38] Once negatively charged, the MSCSs formed a stable suspension in ethanol. Light scattering indicates the mean particle size distribution of MSCSs dispersed in ethanol is ∼487 nm, close to the SEM-determined diameter, demonstrating good dispersion (Figure 1). The electrodes were

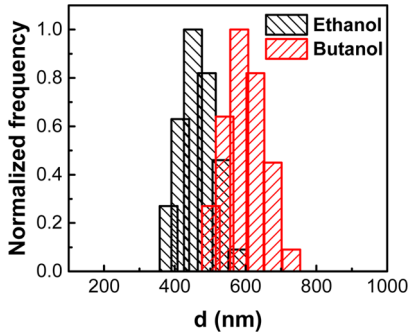

Figure 1. Particle size distributions of MSCSs in ethanol and butanol as determined by dynamic light scattering. The mean diameters of the MSCSs in ethanol and 1-butanol are 487 ± 117 nm and 629 ± 221 nm, respectively (in 1-butanol, clusters are present).

self-assembled on a tilted substrate via slow solvent evaporation (∼24 h) at 40 °C, followed by drying at 150 °C for 1 h to remove any remaining solvents. The combination of monodisperse spheres, the repulsive surface charge, and a stable suspension enabled MSCSs to be self-assembled into a 3D regular array. The ordered and close-packed 3D structure is preserved after drying,[38,39] and no organic binders or other additives are required (Figure 2a,b). The assembly of MSCSs in macroscopic regular array yields an architecture that provides both macropores formed by interstices between MSCSs and the micro- and mesopores of individual MSCSs. This trimodal porous structure provides efficient access of electrolyte to the active sites.[40−42] The significance of the order of the MSCS structure was evaluated by performing comparative tests with

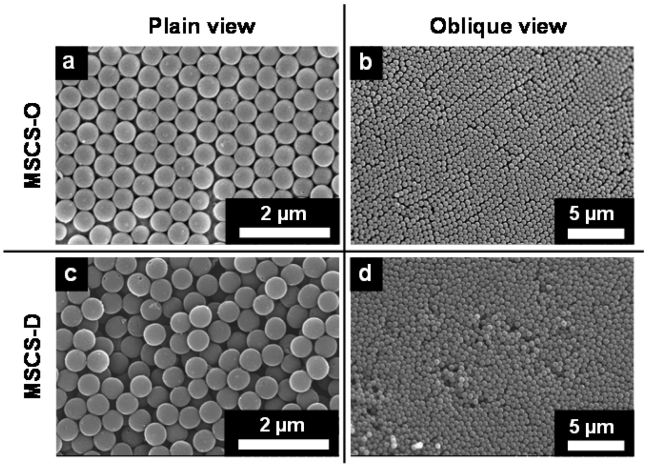

Figure 2. SEM (a, c) plain and (c, d) oblique views of (a, b) MSCS-O and (c, d) MSCS-D.

DOI: 10.1021/acsami.5b01147
ACS Appl. Mater. Interfaces 2015, 7, 9128−9133

3D disordered MSCSs (MSCS-D) electrodes. The MSCS-D electrodes are simply formed by using 1-butanol as the solvent for assembly rather than ethanol. In the less polar 1-butanol, the MSCSs slightly aggregate, and the particle size distribution becomes a bit wider with a peak scattered around 600 nm (Figure 1). The resulting colloidal assemblies (i.e., MSCS-D) remain disordered after drying (Figure 2c,d).

The electrochemical performances of MSCS-O and MSCS-D electrodes were evaluated by CV and GCD measurements in a symmetric two-electrode system. Figure 3a shows the CV

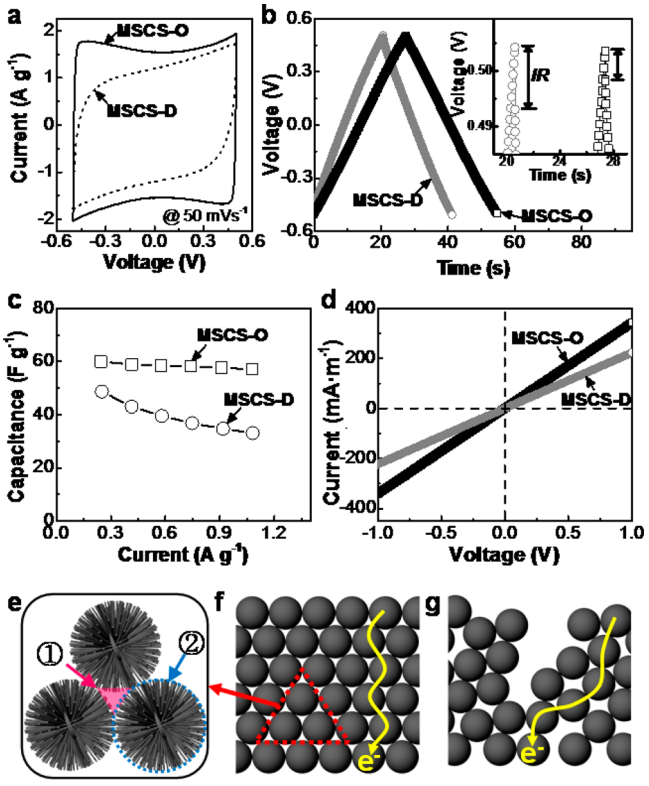

Figure 3. (a) CV curves (scan rate of 50 mV s^{-1}), (b) GCD curves (at 0.58 A g^{-1}) (Inset: enlargement of the peak region of (b) showing the *IR* drop), (c) rate-dependent capacitance, and (d) *I*−*V* curves of MSCS-O and MSCS-D electrodes. Schematic illustrations of (e) the MSCS, (f) MSCS-O, and (g) MSCS-D electrodes and associated electron transport pathways. In (e), the ① macro- and ② meso- and micropores regions of the MSCS electrodes are illustrated.

curves of MSCS-O and MSCS-D electrodes over the voltage window of −0.5 to 0.5 V at a constant scan rate of 50 mV s^{-1}. The MSCS-O electrode retains a nearly rectangular shape with symmetric anodic/cathodic currents (ideal capacitor behavior) during voltage sweeps even at the fast scan rate of 1 V s^{-1} (Supporting Information Figure S4), indicating fast charge propagation across the electrodes.[43,44] The MSCS-D exhibits a distorted CV profile and a decrease in the current values, indicating more resistive behavior. Figure 3b presents the GCD profiles of MSCS electrodes at a constant current of 0.58 A g^{-1}. The voltage−time response of the charging/discharging process for MSCS-O shows a nearly symmetric triangular shape with long charging/discharging durations and a small *IR* drop, confirming an efficient electrical double layer behavior,[45] while MSCS-D shows smaller charging/discharging durations and a larger *IR* drop than MSCS-O. The specific capacitance value of MSCS-O is ∼56 F g^{-1}, which is ∼1.5 times larger than that of MSCS-D, at a current of 0.58 A g^{-1}. The internal resistance calculated from the *IR* drop at the beginning of discharge increases from 6.4 Ω for MSCS-O to 8.8 Ω for MSCS-D. Their differences in specific capacitance values become more significant as current applied increases (Supporting Information Figure S5). Shown in Figure 3c is the rate capability of MSCS electrodes over the current range of 0.25−1.0 A g^{-1}. The initial capacitance of MSCS-O remains as high as 57 F g^{-1} even at a discharge current of 1 A g^{-1}, corresponding to 95% capacity retention, which is rather close to the 60 F g^{-1} at the much lower current density of 0.24 A g^{-1}. At this discharge current, the capacitance drop is more pronounced with 67% retention of initial capacitance for MSCS-D. Figure 3d presents the current−voltage (*I*−*V*) plots of the MSCS-O and MSCS-D electrodes. The electrical conductivity can be directly derived from the slopes of the plots, and it is ∼0.35 S m^{-1} for MSCS-O electrode, larger than ∼0.23 S m^{-1} for MSCS-D electrode.

We attribute the good capacitive and electrical features of MSCS-O to its 3D interconnected conductive network and porous hierarchical nanoarchitecture (Figure 3e,f).[46] Specifically, (i) electrolyte-filled uniform macropores form a continuous phase between carbon spheres that can serve as ion-buffering reservoirs, minimizing the ion diffusion distance into inner pores in all directions.[40,46−49] (ii) Long stretches of carbon walls inside the MSCSs provide straight pore channels, particularly for mesopores, providing an efficient pathway for transporting ions into the inner active sites.[24] (iii) The micropores inside the MSCSs are the primary contributor to the large specific surface area of 1260 m^2 g^{-1} that provides the capacitance.[40,50] (iv) The 3D interconnected structure has a small electrical resistance due to the many contacts between neighboring carbon spheres, which leads to a good electrical conductivity (Figure 3d).[41,51] The disordered sphere network in MSCS-D results in a lower electrical conductivity (Figure 3d), owing to the reduced number of electron transport paths and the longer average path length (Figure 3g). The MSCS-D electrodes also contain a lower volume fraction of active material and excess electrolyte, which does not support a significant electrical double layer,[52] which leads to a drop in the volumetric charge storage capacity. While the performance of SCs is dependent on the electrolyte employed and the associated cation and anion diffusivities and sizes, by using the same electrolyte for both the disordered and ordered systems, the effect of the electrolyte on the relative performance should be minimal. It is important to note that in addition to the good SC performance of MSCS-O, it preserves over 95% of its initial capacitance and exhibits nearly 100% Coulombic efficiency for at least 4000 cycles at a constant current of 0.25 A g^{-1}, indicating a good cycle life (Figure 4).

EIS over a frequency range of 1 × 10^6 to 1 × 10^{-2} Hz was employed to better understand the frequency response characteristics of MSCS electrodes. In Figure 5a,b, the intercept to the real axis (*Z*′) of the Nyquist plots represents an equivalent series resistance that is generally considered the combination of electrode and electrolyte resistances and contact resistance between the current collector and electrode.[5,53] The smaller equivalent series resistance of MSCS-O (4.5 Ω) compared to 7.0 Ω of MSCS-D is ascribed to the good electrical conductivity that comes from the more intimate contact between the MSCSs and shorter electron-transport pathways in the ordered relative to the disordered system (Figure 3f,g). A nearly vertical line at the low-frequency region is observed for MSCS-O, indicating a purely capacitive

DOI: 10.1021/acsami.5b01147
ACS Appl. Mater. Interfaces 2015, 7, 9128−9133

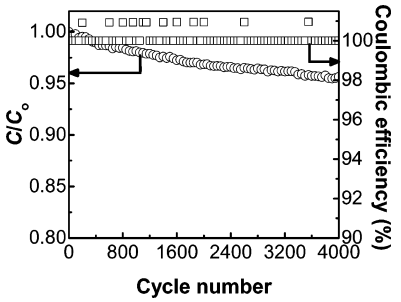

Figure 4. Long-term cycle stability and Coulombic efficiency of MSCS-O during 4000 GCD cycles at a constant current of 0.25 A g^{-1}.

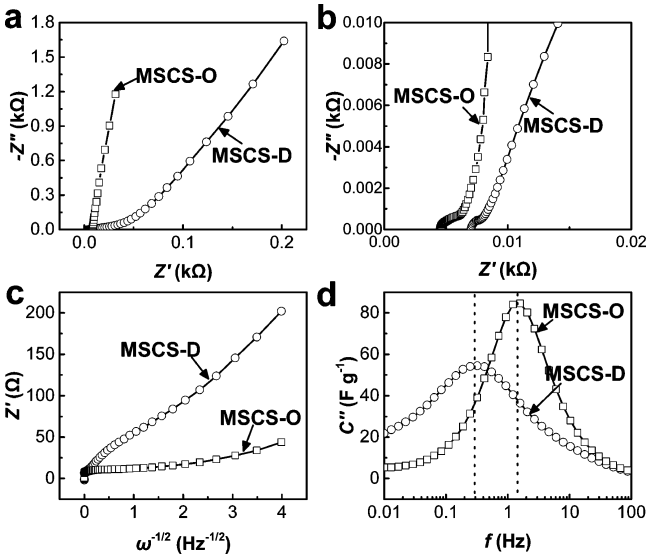

Figure 5. (a) Nyquist plots of MSCS-O and MSCS-D over the frequency range of 100 kHz to 0.01 Hz measured at equilibrium open circuit potential (~0 V). (b) High-frequency region of (a). (c) Randles plot and (d) imaginary part of the capacitance (C'') vs frequency (f) for MSCS-O and MSCS-D. Dotted line indicates the frequency at the peak.

behavior, while MSCS-D becomes more resistive as it tends toward the x-axis of the Nyquist plots (Figure 5a). The low-frequency response is strongly related to the diffusional (or mass transport) behavior of electrochemical systems.[6] Information on ion diffusion into the electrode is also obtained from the impedance in the medium-low frequency region (1–0.01 Hz). The slope of plot of Z' against $\omega^{-1/2}$ (so-called Randles plot, Figure 5c) corresponds to the Warburg coefficient (k_w), which is related to the ion diffusion coefficient (D) as follows:[54,55]

$$k_w = \frac{RT}{n^2F^2A\sqrt{2}}\left(\frac{1}{D^{1/2}C^*}\right) \quad (2)$$

where R is the gas constant, T is the absolute temperature in Kelvin, n is the charge transfer number, A is the area of electrode surface, and C^* is the ionic concentration. The diffusion coefficient of MSCS-O is ~4.64 × 10^{-15} cm^2 s^{-1}, which is larger than the ~2.41 × 10^{-17} cm^2 s^{-1} for MSCS-D. We hypothesize the 3D interconnected and uniform macropore channels of MSCS-O electrode minimize mass transport distances into inner meso- and micropores and thus provide easier accessibility for electrolyte relative to the irregular pores network of the MSCS-D electrode.[6,42,47,56] This finding is further supported by the characteristic relaxation time constant (τ_o), which is defined as the time where the resistive and capacitive behaviors are equal (Figure 5d) for the two systems.[57,58] τ_o is determined from the complex form of capacitance, $C(\omega)$, which can be obtained from frequency-dependent impedance $Z(\omega)$ in eqs 3, 4, and 5.[58]

$$Z(\omega) = 1/j\omega C(\omega) \quad (3)$$

$$Z(\omega) = Z'(\omega) + jZ''(\omega) \quad (4)$$

$$C'(\omega) = \frac{-Z''(\omega)}{\omega|Z(\omega)|^2},\ C''(\omega) = \frac{Z'(\omega)}{w|Z(\omega)|^2} \quad (5)$$

ω is the angular frequency (= $2\pi f$), and $C'(\omega)$ and $C''(\omega)$ are the real part and imaginary parts of $C(\omega)$, respectively. $\tau_o = 1/f_0$ where f_0 is the frequency at the half-maximum of $C'(\omega)$ or peak maximum of $C''(\omega)$. The peak maximum of $C''(\omega)$ for MSCS-O appears at a significantly higher frequency than that of MSCS-D, reflecting the 0.69 s τ_o for MSCS-O compared to 3.11 s for MSCS-D. The rapid frequency-response indicates the efficient mass transport of the well-defined porous structure of MSCS-O,[56,59] additionally supporting the hypothesis that the MSCS-O electrode exhibits fast charging/discharging kinetics and a high capacity even at high current densities because of both the good electrode electrical conductivity of the ordered structure, and efficient ion transport through the 3D interconnected macropores.

CONCLUSION

In summary, we demonstrate the impact of ordering on the nanostructured supercapacitor electrode that contains a carefully determined micro- meso-, and macropore structure. By changing only the solvent used for assembly, MSCSs that serve as the basis of the electrode can be assembled into either a close-packed periodic (a colloidal crystal) or disordered architecture (a colloidal glass). The hierarchically ordered structure, in which both the electron- and ion-transport pathways are continuous, provides good electron mobility and ion diffusion even at relatively high current densities, enabling high rate capability. The absence of binder and other additive materials in the electrodes is also probably important, as such materials may impede efficient ion and electron conductivity by blocking some of the electron- and ion-conduction pathways.

ASSOCIATED CONTENT

Supporting Information

Discussion and characterization of MSCS electrodes with BET, zeta potential, Nyquist plots, rate-dependent capacitance, TGA in air, and electrochemical tests (CV and GCD). This material is available free of charge via the Internet at http://pubs.acs.org.

AUTHOR INFORMATION

Corresponding Authors

*E-mail: (K.Y.) k-yano@mosk.tytlabs.co.jp.
*E-mail: (P.V.B.) pbraun@illinois.edu.

Author Contributions

⊥These authors contributed equally to this work.

Notes

The authors declare no competing financial interest.

DOI: 10.1021/acsami.5b01147
ACS Appl. Mater. Interfaces 2015, 7, 9128–9133

■ ACKNOWLEDGMENTS

This work was supported by Toyota Central R&D Laboratories (MSCS colloid fabrication and electrode fabrication) and the U.S. Department of Energy, Office of Basic Energy Sciences, Division of Materials Sciences and Engineering under Award No. DE-FG02-07ER46471 (electrochemical testing and modeling), through the Frederick Seitz Materials Research Laboratory at the Univ. of Illinois at Urbana−Champaign. This work was performed in part in the Frederick Seitz Materials Research Laboratory Central Research Facilities, Univ. of Illinois.

■ REFERENCES

(1) Gogotsi, Y. Materials Science: Energy Storage Wrapped up. *Nature* **2014**, *509*, 568−570.
(2) Kaempgen, M.; Chan, C. K.; Ma, J.; Cui, Y.; Gruner, G. Printable Thin Film Supercapacitors Using Single-Walled Carbon Nanotubes. *Nano Lett.* **2009**, *9*, 1872−1876.
(3) Yoo, J. J.; Balakrishnan, K.; Huang, J.; Meunier, V.; Sumpter, B. G.; Srivastava, A.; Conway, M.; Mohana Reddy, A. L.; Yu, J.; Vajtai, R.; Ajayan, P. M. Ultrathin Planar Graphene Supercapacitors. *Nano Lett.* **2011**, *11*, 1423−1427.
(4) Chabi, S.; Peng, C.; Hu, D.; Zhu, Y. Ideal Three-Dimensional Electrode Structures for Electrochemical Energy Storage. *Adv. Mater.* **2014**, *26*, 2440−2445.
(5) Chmiola, J.; Yushin, G.; Gogotsi, Y.; Portet, C.; Simon, P.; Taberna, P. L. Anomalous Increase in Carbon Capacitance at Pore Sizes Less Than 1 Nanometer. *Science* **2006**, *313*, 1760−1763.
(6) Wang, D.-W.; Li, F.; Fang, H.-T.; Liu, M.; Lu, G.-Q.; Cheng, H.-M. Effect of Pore Packing Defects in 2-D Ordered Mesoporous Carbons on Ionic Transport. *J. Phys. Chem. B* **2006**, *110*, 8570−8575.
(7) Wang, D.-W.; Li, F.; Liu, M.; Lu, G. Q.; Cheng, H.-M. 3D Aperiodic Hierarchical Porous Graphitic Carbon Material for High-Rate Electrochemical Capacitive Energy Storage. *Angew. Chem., Int. Ed.* **2008**, *47*, 373−376.
(8) Long, J. W.; Dunn, B.; Rolison, D. R.; White, H. S. Three-Dimensional Battery Architectures. *Chem. Rev.* **2004**, *104*, 4463−4492.
(9) Lee, K. T.; Lytle, J. C.; Ergang, N. S.; Oh, S. M.; Stein, A. Synthesis and Rate Performance of Monolithic Macroporous Carbon Electrodes for Lithium-Ion Secondary Batteries. *Adv. Funct. Mater.* **2005**, *15*, 547−556.
(10) Korenblit, Y.; Rose, M.; Kockrick, E.; Borchardt, L.; Kvit, A.; Kaskel, S.; Yushin, G. High-Rate Electrochemical Capacitors Based on Ordered Mesoporous Silicon Carbide-Derived Carbon. *ACS Nano* **2010**, *4*, 1337−1344.
(11) Stoller, M. D.; Park, S.; Zhu, Y.; An, J.; Ruoff, R. S. Graphene-Based Ultracapacitors. *Nano Lett.* **2008**, *8*, 3498−3502.
(12) Wang, Y.; Shi, Z.; Huang, Y.; Ma, Y.; Wang, C.; Chen, M.; Chen, Y. Supercapacitor Devices Based on Graphene Materials. *J. Phys. Chem. C* **2009**, *113*, 13103−13107.
(13) Liu, C.; Yu, Z.; Neff, D.; Zhamu, A.; Jang, B. Z. Graphene-Based Supercapacitor with an Ultrahigh Energy Density. *Nano Lett.* **2010**, *10*, 4863−4868.
(14) Yoon, S.; Lee, J.; Hyeon, T.; Oh, S. M. Electric Double-Layer Capacitor Performance of a New Mesoporous Carbon. *J. Electrochem. Soc.* **2000**, *147*, 2507−2512.
(15) Tabata, S.; Isshiki, Y.; Watanabe, M. Inverse Opal Carbons Derived from a Polymer Precursor as Electrode Materials for Electric Double-Layer Capacitors. *J. Electrochem. Soc.* **2008**, *155*, K42−K49.
(16) Moriguchi, I.; Nakahara, F.; Furukawa, H.; Yamada, H.; Kudo, T. Colloidal Crystal-Templated Porous Carbon as a High Performance Electrical Double-Layer Capacitor Material. *Electrochem. Solid-State Lett.* **2004**, *7*, A221−A223.
(17) Schuster, J.; He, G.; Mandlmeier, B.; Yim, T.; Lee, K. T.; Bein, T.; Nazar, L. F. Spherical Ordered Mesoporous Carbon Nanoparticles with High Porosity for Lithium−Sulfur Batteries. *Angew. Chem., Int. Ed.* **2012**, *51*, 3591−3595.
(18) Weng, Z.; Su, Y.; Wang, D.-W.; Li, F.; Du, J.; Cheng, H.-M. Graphene−Cellulose Paper Flexible Supercapacitors. *Adv. Energy Mater.* **2011**, *1*, 917−922.
(19) Jost, K.; Perez, C. R.; McDonough, J. K.; Presser, V.; Heon, M.; Dion, G.; Gogotsi, Y. Carbon Coated Textiles for Flexible Energy Storage. *Energy Environ. Sci.* **2011**, *4*, 5060−5067.
(20) Meng, C.; Liu, C.; Chen, L.; Hu, C.; Fan, S. Highly Flexible and All-Solid-State Paperlike Polymer Supercapacitors. *Nano Lett.* **2010**, *10*, 4025−4031.
(21) Kang, Y. J.; Chun, S.-J.; Lee, S.-S.; Kim, B.-Y.; Kim, J. H.; Chung, H.; Lee, S.-Y.; Kim, W. All-Solid-State Flexible Supercapacitors Fabricated with Bacterial Nanocellulose Papers, Carbon Nanotubes, and Triblock-Copolymer Ion Gels. *ACS Nano* **2012**, *6*, 6400−6406.
(22) Chen, W.; Rakhi, R. B.; Hu, L.; Xie, X.; Cui, Y.; Alshareef, H. N. High-Performance Nanostructured Supercapacitors on a Sponge. *Nano Lett.* **2011**, *11*, 5165−5172.
(23) Zhou, C.; Zhang, Y.; Li, Y.; Liu, J. Construction of High-Capacitance 3D CoO@Polypyrrole Nanowire Array Electrode for Aqueous Asymmetric Supercapacitor. *Nano Lett.* **2013**, *13*, 2078−2085.
(24) Wang, Y. G.; Li, H. Q.; Xia, Y. Y. Ordered Whiskerlike Polyaniline Grown on the Surface of Mesoporous Carbon and Its Electrochemical Capacitance Performance. *Adv. Mater.* **2006**, *18*, 2619−2623.
(25) Cui, C.; Qian, W.; Yu, Y.; Kong, C.; Yu, B.; Xiang, L.; Wei, F. Highly Electroconductive Mesoporous Graphene Nanofibers and Their Capacitance Performance at 4 V. *J. Am. Chem. Soc.* **2014**, *136*, 2256−2259.
(26) Zhang, H.; Yu, X.; Braun, P. V. Three-Dimensional Bicontinuous Ultrafast-Charge and -Discharge Bulk Battery Electrodes. *Nat. Nanotechnol.* **2011**, *6*, 277−281.
(27) Pikul, J. H.; Gang Zhang, H.; Cho, J.; Braun, P. V.; King, W. P. High-Power Lithium Ion Microbatteries from Interdigitated Three-Dimensional Bicontinuous Nanoporous Electrodes. *Nat. Commun.* **2013**, *4*, 1732.
(28) Lee, S. W.; Yabuuchi, N.; Gallant, B. M.; Chen, S.; Kim, B.-S.; Hammond, P. T.; Shao-Horn, Y. High-Power Lithium Batteries from Functionalized Carbon-Nanotube Electrodes. *Nat. Nanotechnol.* **2010**, *5*, 531−537.
(29) Xu, Y.; Sheng, K.; Li, C.; Shi, G. Self-Assembled Graphene Hydrogel via a One-Step Hydrothermal Process. *ACS Nano* **2010**, *4*, 4324−4330.
(30) Yin, S.; Zhang, Y.; Kong, J.; Zou, C.; Li, C. M.; Lu, X.; Ma, J.; Boey, F. Y. C.; Chen, X. Assembly of Graphene Sheets into Hierarchical Structures for High-Performance Energy Storage. *ACS Nano* **2011**, *5*, 3831−3838.
(31) Pushparaj, V. L.; Shaijumon, M. M.; Kumar, A.; Murugesan, S.; Ci, L.; Vajtai, R.; Linhardt, R. J.; Nalamasu, O.; Ajayan, P. M. Flexible Energy Storage Devices Based on Nanocomposite Paper. *Proc. Natl. Acad. Sci. U. S. A* **2007**, *104*, 13574−13577.
(32) Niu, Z.; Chen, J.; Hng, H. H.; Ma, J.; Chen, X. A Leavening Strategy to Prepare Reduced Graphene Oxide Foams. *Adv. Mater.* **2012**, *24*, 4144−4150.
(33) Raymundo-Piñero, E.; Leroux, F.; Béguin, F. A High-Performance Carbon for Supercapacitors Obtained by Carbonization of a Seaweed Biopolymer. *Adv. Mater.* **2006**, *18*, 1877−1882.
(34) Zhang, L. L.; Zhao, X. S. Carbon-Based Materials as Supercapacitor Electrodes. *Chem. Soc. Rev.* **2009**, *38*, 2520−2531.
(35) Frackowiak, E. Carbon Materials for Supercapacitor Application. *Phys. Chem. Chem. Phys.* **2007**, *9*, 1774−1785.
(36) Tatsuda, N.; Yano, K. Pore Size Control of Monodispersed Starburst Carbon Spheres. *Carbon* **2013**, *51*, 27−35.
(37) Nakamura, T.; Yamada, Y.; Yano, K. Monodispersed Nanoporous Starburst Carbon Spheres and Their Three-Dimensionally Ordered Arrays. *Microporous Mesoporous Mater.* **2009**, *117*, 478−485.
(38) Goodman, M. D.; Arpin, K. A.; Mihi, A.; Tatsuda, N.; Yano, K.; Braun, P. V. Enabling New Classes of Templated Materials through Mesoporous Carbon Colloidal Crystals. *Adv. Opt. Mater.* **2013**, *1*, 300−304.

DOI: 10.1021/acsami.5b01147
ACS Appl. Mater. Interfaces 2015, 7, 9128−9133

(39) Stöber, W.; Fink, A.; Bohn, E. Controlled Growth of Monodisperse Silica Spheres in the Micron Size Range. *J. Colloid Interface Sci.* **1968**, *26*, 62−69.
(40) Duay, J.; Sherrill, S. A.; Gui, Z.; Gillette, E.; Lee, S. B. Self-Limiting Electrodeposition of Hierarchical MnO_2 and $M(OH)_2/MnO_2$ Nanofibril/Nanowires: Mechanism and Supercapacitor Properties. *ACS Nano* **2013**, *7*, 1200−1214.
(41) Wang, Z.-L.; Xu, D.; Wang, H.-G.; Wu, Z.; Zhang, X.-B. In Situ Fabrication of Porous Graphene Electrodes for High-Performance Energy Storage. *ACS Nano* **2013**, *7*, 2422−2430.
(42) Wu, Z.-S.; Winter, A.; Chen, L.; Sun, Y.; Turchanin, A.; Feng, X.; Müllen, K. Three-Dimensional Nitrogen and Boron Co-doped Graphene for High-Performance All-Solid-State Supercapacitors. *Adv. Mater.* **2012**, *24*, 5130−5135.
(43) Kim, S.-K.; Kim, Y. K.; Lee, H.; Lee, S. B.; Park, H. S. Superior Pseudocapacitive Behavior of Confined Lignin Nanocrystals for Renewable Energy-Storage Materials. *ChemSusChem* **2014**, *7*, 1094−1101.
(44) Xu, Z.; Li, Z.; Holt, C. M. B.; Tan, X.; Wang, H.; Amirkhiz, B. S.; Stephenson, T.; Mitlin, D. Electrochemical Supercapacitor Electrodes from Sponge-like Graphene Nanoarchitectures with Ultrahigh Power Density. *J. Phys. Chem. Lett.* **2012**, *3*, 2928−2933.
(45) Kim, S.-K.; Koo, H.-J.; Lee, A.; Braun, P. V. Selective Wetting-Induced Micro-electrode Patterning for Flexible Micro-supercapacitors. *Adv. Mater.* **2014**, *26*, 5108−5112.
(46) Fan, L. Z.; Hu, Y. S.; Maier, J.; Adelhelm, P.; Smarsly, B.; Antonietti, M. High Electroactivity of Polyaniline in Supercapacitors by Using a Hierarchically Porous Carbon Monolith as a Support. *Adv. Funct. Mater.* **2007**, *17*, 3083−3087.
(47) Li, Y.; Li, Z.; Shen, P. K. Simultaneous Formation of Ultrahigh Surface Area and Three-Dimensional Hierarchical Porous Graphene-Like Networks for Fast and Highly Stable Supercapacitors. *Adv. Mater.* **2013**, *25*, 2474−2480.
(48) Chen, J.; Yano, K. Highly Monodispersed Tin Oxide/Mesoporous Starbust Carbon Composite as High-Performance Li-Ion Battery Anode. *ACS Appl. Mater. Interfaces* **2013**, *5*, 7682−7687.
(49) Lee, G.-J.; Pyun, S.-I. Theoretical Approach to Ion Penetration into Pores with Pore Fractal Characteristics during Double-Layer Charging/Discharging on a Porous Carbon Electrode. *Langmuir* **2006**, *22*, 10659−10665.
(50) Dubal, D. P.; Lee, S. H.; Kim, J. G.; Kim, W. B.; Lokhande, C. D. Porous Polypyrrole Clusters Prepared by Electropolymerization for a High Performance Supercapacitor. *J. Mater. Chem.* **2012**, *22*, 3044−3052.
(51) Yang, X.; Zhu, J.; Qiu, L.; Li, D. Bioinspired Effective Prevention of Restacking in Multilayered Graphene Films: Towards the Next Generation of High-Performance Supercapacitors. *Adv. Mater.* **2011**, *23*, 2833−2838.
(52) Miller, J. R.; Simon, P. Electrochemical Capacitors for Energy Management. *Science* **2008**, *321*, 651−652.
(53) Shaijumon, M. M.; Ou, F. S.; Ci, L.; Ajayan, P. M. Synthesis of Hybrid Nanowire Arrays and Their Application as High Power Supercapacitor Electrodes. *Chem. Commun.* **2008**, 2373−2375.
(54) Hwang, K. S.; Yoon, T. H.; Lee, C. W.; Son, Y. S.; Hwang, J. K. Discharge−Charge Characteristics and Performance of Li/FeOOH-(an) Battery with PAN-Based Polymer Electrolyte. *J. Power Sources* **1998**, *75*, 13−18.
(55) Hsieh, C.-T.; Hsu, S.-M.; Lin, J.-Y.; Teng, H. Electrochemical Capacitors Based on Graphene Oxide Sheets Using Different Aqueous Electrolytes. *J. Phys. Chem. C* **2011**, *115*, 12367−12374.
(56) Choi, B. G.; Yang, M.; Hong, W. H.; Choi, J. W.; Huh, Y. S. 3D Macroporous Graphene Frameworks for Supercapacitors with High Energy and Power Densities. *ACS Nano* **2012**, *6*, 4020−4028.
(57) Pech, D.; Brunet, M.; Durou, H.; Huang, P.; Mochalin, V.; Gogotsi, Y.; Taberna, P.-L.; Simon, P. Ultrahigh-Power Micrometre-Sized Supercapacitors Based on Onion-Like Carbon. *Nat. Nanotechnol.* **2010**, *5*, 651−654.
(58) Taberna, P. L.; Simon, P.; Fauvarque, J. F. Electrochemical Characteristics and Impedance Spectroscopy Studies of Carbon-Carbon Supercapacitors. *J. Electrochem. Soc.* **2003**, *150*, A292−A300.
(59) Lu, X.; Yu, M.; Zhai, T.; Wang, G.; Xie, S.; Liu, T.; Liang, C.; Tong, Y.; Li, Y. High Energy Density Asymmetric Quasi-Solid-State Supercapacitor Based on Porous Vanadium Nitride Nanowire Anode. *Nano Lett.* **2013**, *13*, 2628−2633.

DOI: 10.1021/acsami.5b01147
ACS Appl. Mater. Interfaces 2015, 7, 9128−9133